PROCEEDINGS OF SCIENCE

# Numerical simulation of Dirac semimetals

**V. V. Braguta**
*Institute of Theoretical and Experimental Physics, 117259 Moscow, Russia*
*E-mail:* braguta@itep.ru

**M. I. Katsnelson**
*Radboud University, Institute for Molecules and Materials, NL-6525AJ Nijmegen, The Netherlands*
*E-mail:* m.katsnelson@science.ru.nl

**A. Yu. Kotov***
*Institute of Theoretical and Experimental Physics, 117259 Moscow, Russia*
*E-mail:* kotov@itep.ru

**A. A. Nikolaev**
*Far Eastern Federal University, School of Biomedicine, 690950 Vladivostok, Russia*
*E-mail:* nikolaev.aa@dvfu.ru

Dirac semimetals are recently discovered materials with low energy electronic excitation spectrum similar to the massless two favour 3+1 Dirac fermions. The interaction between quasiparticles in Dirac semimetals is instantaneous Coulomb with large effective coupling constant $\alpha \sim 1$. In this report we present results of study of the phase diagram of Dirac semimetals within lattice simulation with rooted staggered fermions. In particular, we calculate the chiral condensate as a function of effective coupling constant and Fermi velocity anisotropy and thus determine the position of semimetal-insulator transition in Dirac semimetals.

*34th annual International Symposium on Lattice Field Theory*
*24-30 July 2016*
*University of Southampton, UK*

*Speaker.





PoS(LATTICE2016)243

## 1. Introduction

One of the most important recent advances in the condensed matter physics is the experimental discovery of graphene [1, 2]. The main peculiarity of graphene, which attracts considerable interest, is the existence of two Fermi points in its electronic spectrum. In the vicinity of the Fermi points fermionic excitations are analogous to massless $2D$ Dirac fermions [3].

Recently there have been discovered Dirac semimetals $Na_3Bi$ [4] and $Cd_3As_2$ [5, 6], which are $3D$ analogues of graphene. These materials also have two Fermi points. In the vicinity of these points fermionic excitations are analogous to massless $3D$ Dirac fermions and the dispersion relation can be written as $E^2 = v_\parallel^2(k_x^2+k_y^2)+v_\perp^2 k_z^2$, where $v_\parallel, v_\perp$ are Fermi velocities in the $(x,y)$-plane and $z$-direction correspondingly. Fermi velocities for these Dirac semimetals are $v_f \sim c/1000$.

Fermionic excitations in the Dirac semimetals interact with each other via electromagnetic interaction. The smallness of Fermi velocity allows to disregard the effects of retardation and magnetic interaction. In other words, one can treat interaction between quasiparticles as Coulomb instantaneous. Effective coupling constant $\alpha_{eff} = \alpha_{el}/v_f > 1$, where $\alpha_{el} = 1/137$ is the coupling constant of electromagnetic interaction. One sees that the effective coupling constant is large enough and can significantly change the properties of Dirac semimetals. In particular, it is known, that large interaction between quasiparticles can lead to dynamical chiral symmetry breaking, appearance of the gap in the fermionic spectrum and phase transition from semimetal to insulator.

Our purpose is the study of the phase diagram of Dirac semimetals within Monte-Carlo simulations. In particular, we study the value of the critical coupling constant $\alpha_{eff}^c$, at which the transition from semimetal to insulator occurs, and its dependence on the value of Fermi velocity anisotropy $\xi = v_\parallel/v_\perp$. We are going to use Monte-Carlo simulation which fully accounts many-body effects for arbitrary coupling constant. This approach proved to be very efficient in studying the properties of the strongly correlated systems, for instance, graphene [7, 8, 9]. A more complete description of this study is given in [10]. It is worth mentioning that the phase diagram of Dirac semimetals was studied analytically in [11, 12, 13, 14, 15].

## 2. Effective model

The partition function of the system to study:

$$Z = \int D\psi\, D\bar{\psi}\, DA_4\, \exp\left(-S_E\right), \tag{2.1}$$

where $\bar{\psi}, \psi$ are fermionic fields, $A_4$ - is the timelike component of the electromagnetic vector potential. Euclidean action $S_E$ can be written in the following form:

$$S_E = \sum_{a=1}^{N_f=2} \int d^3x dt\, \bar{\psi}_a(\gamma_4(\partial_4 + iA_4) + \xi_i\gamma_i\partial_i)\psi_a + \frac{1}{8\pi\alpha_{eff}}\int d^3x dt\,(\partial_i A_4)^2 \tag{2.2}$$

Here $\xi_i \sim 1$ are factors that incorporate Fermi velocity anisotropy. Note that action (2.2) doesn't depend on spacelike components $A_i$. Taking into account spacelike components of the vector potential leads to correction suppressed by factors $\sim (v_f)^k$, $k > 1$, which study is beyond the approximation used in our simulations.

In the study we used noncompact discretization of electromagnetic field:

$$S_g = \frac{\beta}{2}\sum_{x,i}(\theta_4(x)-\theta_4(x+i))^2, \tag{2.3}$$

where we introduced $\beta = \frac{1}{4\pi\alpha_{eff}}$.

We used staggered fermions [16] with rooting for modelling $N_f = 2$ fermionic flavours:

$$S_f = \bar{\Psi}_x D_{x,y}\Psi_y = \sum_x \Bigg( m\bar{\Psi}_x\Psi_x + \frac{1}{2}[\bar{\Psi}_x\eta_4(x)e^{i\theta_4(x)}\Psi_{x+\hat{4}} - \bar{\Psi}_{x+4}\eta_4(x)e^{-i\theta_4(x)}\Psi_x] + \\ + \frac{1}{2}\sum_{i=1}^{3}\xi_i[\bar{\Psi}_x\eta_i(x)\Psi_{x+\hat{i}} - \bar{\Psi}_{x+i}\eta_i(x)\Psi_x]\Bigg), \tag{2.4}$$

where $\eta_\mu(x) = (-1)^{x_1+\ldots+x_{\mu-1}}$, $\mu = 1,\ldots,4$ ($\eta_1 = 1$) are factors corresponding to $\gamma$-matrices for staggered fermions.

We introduced nonzero mass in Eq. (2.4) for invertibility of the Dirac operator $D_{x,y}$. Results for zero mass are obtained by studying the extrapolation to the chiral limit $m \to 0$.

Integrating over fermionic fields, one obtains

$$Z = \int D\theta_4(x)\exp\left(-S_{eff}\right), \qquad S_{eff} = -\ln\det D[\theta] + S_g. \tag{2.5}$$

The effective action (2.5) corresponds to four Dirac fermions in the continuum limit [16]. In order to have two fermions one has to take the second root of the determinant of the Dirac operator, which is realized by the rooting procedure. Thus, the effective action, which was used for the study, has the following form:

$$S^{(eff)} = -\frac{1}{2}\ln\det D[\theta] + S_g. \tag{2.6}$$

For the generation of $\theta_4(x)$ field configurations with the statistical weight $\exp(-S^{(eff)}[\theta])$ we used rational hybrid Monte-Carlo method [16].

It is known that strong enough interaction between quasiparticles can lead to the chiral symmetry breaking, formation of the condensate $\bar{\Psi}\Psi$ and appearance of the gap in the spectrum. We study the dependence of the chiral condensate on the value of $\alpha_{eff}$, which is the order parameter of the transition semimetal-insulator. In our study we look at the following observables: fermionic condensate $\sigma = \bar{\Psi}\Psi$, susceptibility of the chiral condensate $\chi = \frac{\partial\sigma}{\partial m}$[1], logarithmic derivative of the chiral condensate $R = \frac{\partial\ln\sigma}{\partial\ln m}$.

Note that in the chiral limit $m = 0$: $\sigma = 0$ in the chiral symmetric phase and $\sigma \neq 0$ in the phase where chiral symmetry is broken. The logarithmic derivative $R$ reveals the following properties: in the chirally symmetric phase $\sigma \sim m$ and $R \to 1$. At the critical point $R \to 1/\delta$, where $\delta$ is a universal critical exponent and $R \to 0$ in the phase with broken chiral symmetry.

## 3. Numerical results

First let us study the case without anisotropy of Fermi velocity in different directions ($\xi_1 = \xi_2 = \xi_3 = 1$). In numerical simulations we used lattice size $20^4$.

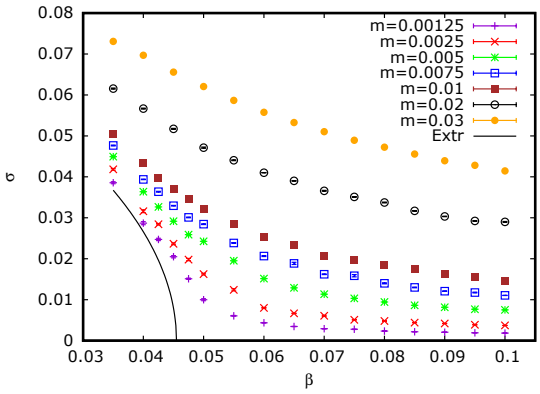


**Figure 1:** The chiral condensate $\langle\bar{\Psi}\Psi\rangle$ as a function of $\beta$ for different values of mass $m$. Black line corresponds to chiral limit $m \to 0$ taken with the help of EoS (3.1).

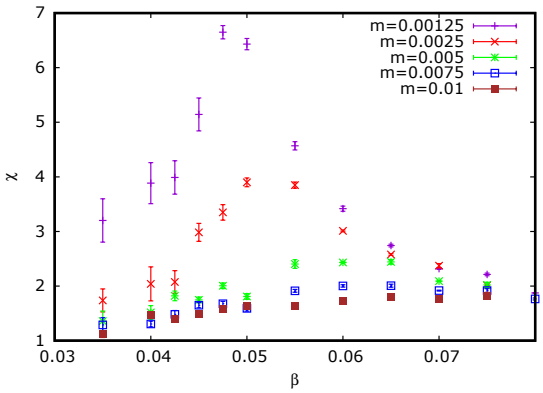


**Figure 2:** Susceptibility $\chi$ of the chiral condensate as a function of $\beta$ for different values of mass $m$.

In Fig. 1 the dependence of $\sigma$ on $\beta$ for different fermion masses is presented. It is seen from this plot that the chiral condensate is nonzero at $\beta < \beta_c$ with critical value $\beta_c \sim 0.04 - 0.06$.

In Fig. 2 we present results for the susceptibility of the chiral condensate $\chi = \frac{\partial\sigma}{\partial m}$ as a function of $\beta$ for different values of mass. The plot shows a clear peak at small values of mass $m \leq 0.005$, which is also an indication of the phase transition. The critical value of the $\beta$ determined from the position of the peak is slightly larger and decreases when the mass decreases.

In Fig.3 the dependence of the logarithmic derivative $R$ as a function of mass for different values of $\beta$ is presented. Taking into account the behaviour of the derivative discussed above one can conclude that for large values of $\beta \geq 0.0475$ the system has no gap, while for small values of $\beta \leq 0.0425$ results indicate the formation of the gap. Thus we can estimate the critical coupling $\beta = 0.0450 \pm 0.0025$, which is in the agreement with the previous estimations obtained with the help of the chiral condensate and susceptibility.

To estimate the values of $\beta_c$ more precisely we fit the data with an equation of state (EoS):

$$mX(\beta) = Y(\beta) f_1(\sigma) + f_3(\sigma), \tag{3.1}$$

[1]Note, that all dimensionful parameters and observables in this paper are expressed in lattice units

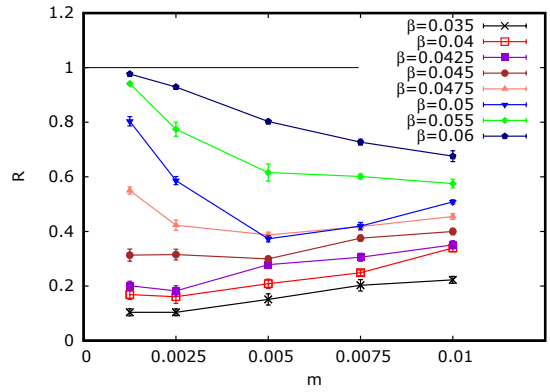


**Figure 3:** Logarithmic derivative of $R$ of the chiral condensate as a function of mass $m$ for different values of coupling constant $\beta$.

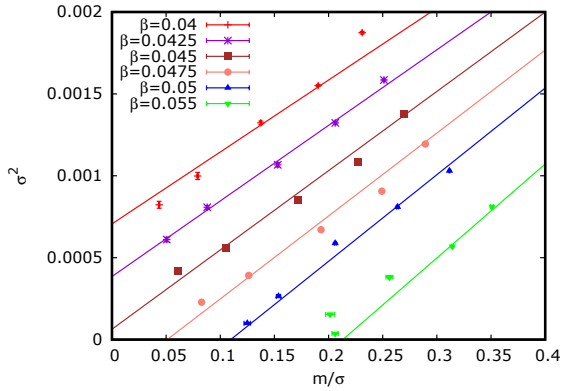


**Figure 4:** The squared chiral condensate $\sigma$ as a function of $\frac{m}{\sigma}$. Straight lines correspond to the fit of all points with EoS (3.1).

| $\xi$ | $\alpha^c_{eff}$ |
|---|---|
| 1 | 1.749(2) |
| 0.5 | 1.762(3) |
| 0.2 | 1.467(10) |
| 0.1 | 1.150(8) |

**Table 1:** Critical coupling constant $\alpha^c_{eff}$ as a function of Fermi velocity anisotropy $\xi$.

where $X(\beta)$ and $Y(\beta)$ are expanded in the vicinity of critical $\beta_c$: $X(\beta) = X_0 + X_1(1-\beta/\beta_c)$, $Y(\beta) = Y_1(1-\beta/\beta_c)$. For functions $f_1$ and $f_3$ we used classical critical exponents: $f_1(\sigma) = \sigma$, $f_3(\sigma) = \sigma^3$. This equation of state can be easily visualized if one plots $\sigma^2$ vs $m/\sigma$ (Fisher plot). The resulting dependence $\sigma^2(m/\sigma)$ forms straight lines for different $\beta$. The line that crosses the origin corresponds to $\beta_c$. The Fisher plot is presented in Fig. 4. Straight lines correspond to the fit by Eq. 3.1. This fit gives $\beta_c = 0.04549(6)$, what corresponds to critical coupling $\alpha^c_{eff} = 1.749(2)$. Here only statistical error is given. Note that the obtained value is close to the results, obtained within ladder approximation [13].

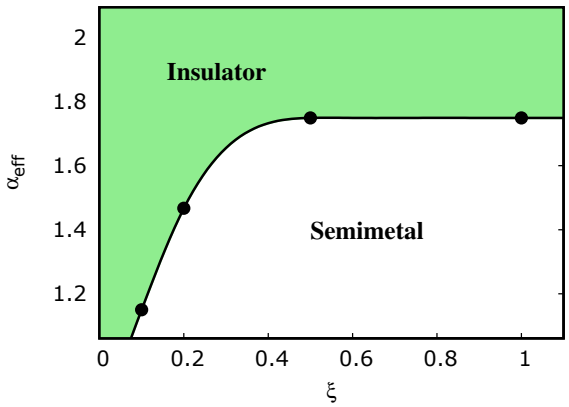


**Figure 5:** The dependence of the critical coupling constant $\alpha^c_{eff}$ on the Fermi velocity anisotropy $\xi$. For $\alpha_{eff} > \alpha^c_{eff}(\xi)$ the system is in the insulator phase. Smaller values of $\alpha_{eff} < \alpha^c_{eff}(\xi)$ correspond to the semimetal phase. Statistical errors are smaller than data points. Lines are to guide the eyes.

Now we proceed to the anisotropic case which is parametrized by the parameter $\xi = \xi_3 < 1$ ($\xi_1 = \xi_2 = 1$). The calculations were carried out with the lattice size $20^4$. We considered the values of $\xi = 0.1, 0.2, 0.5$. The figures for these values of $\xi$ are similar to the isotropic case, for this reason we do not show it here. The resulting dependence of the critical $\beta_c$ on the value of $\xi$ is presented in Tab. 1 and shown in the Fig. 5.

Parameter $\xi$ effectively controls the dimensionality of the system. If $\xi = 1$ the system is 3-dimensional. If $\xi = 0$ the system corresponds to the stack of 2-dimensional sheets with Fermi velocity $v_{\|}$. From quantum mechanics one may expect that for the 2D system the critical coupling is smaller, what is in agreement with the presented results.

The effective coupling constants for the Dirac semimetals $Na_3Bi$, $Cd_3As_2$ are $\alpha_{eff} \sim 5$. Our analysis implies that these materials are deep in the insulator phase, what contradicts to the experiments. It rises very important question: why such strong interaction in Dirac semimetals does not lead to the generation of energy gap in the fermion spectrum? This puzzle probably can be settled either by renormalization effects or by the fact that in the real world the interaction potential is screened by bound electrons. Although this question is very important it is beyond the scope of this report.

## 4. Conclusions

The phase diagram of Dirac semimetals was studied within lattice Monte-Carlo simulation. We concentrated on the dynamical chiral symmetry breaking which results in semimetal/insulator transition. We measured the chiral condensate and the chiral susceptibility for different values of the fermion mass, effective coupling constant and Fermi velocity anisotropy. We determined the values of the critical coupling of the semimetal/insulator transition for different values of the Fermi velocity anisotropy. Tentative phase diagram of Dirac semimetals is drawn.

It turns out that within the Dirac model with Coulomb interaction both $Na_3Bi$ and $Cd_3As_2$ known experimentally to be Dirac semimetals would lie deeply in the insulating region of the

phase diagram. It probably shows a decisive role of screening of the interelectron interaction in real materials, similar to the situation in graphene.

## Acknowledgements

The authors are grateful to M.A. Zubkov, who drew their attention to the considered problem. The authors thank I.A. Shovkovy, Z.V. Khaidukov for useful discussions and comments. Numerical simulations were carried out on GPU cluster of the federal center for collective usage at NRC "Kurchatov Institute" (http://computing.kiae.ru/).

## References

[1] K. S. Novoselov *et al.*, Electric field effect in atomically thin carbon films. *Science*, 306(5696):666–669, 2004.

[2] A. K. Geim and K. S. Novoselov, The rise of graphene. *Nat Mater*, 6(3):183–191, Mar 2007.

[3] K. S. Novoselov *et al.*, Two-dimensional gas of massless dirac fermions in graphene. *Nature*, 438(7065):197–200, Nov 2005.

[4] Z. K. Liu *et al.*, Discovery of a three-dimensional topological dirac semimetal, na3bi. *Science*, 343(6173):864–867, 2014.

[5] Madhab Neupane *et al.*, Observation of a three-dimensional topological dirac semimetal phase in high-mobility cd3as2. *Nat Commun*, 5, May 2014.

[6] Sergey Borisenko *et al.*, Experimental realization of a three-dimensional dirac semimetal. *Phys. Rev. Lett.*, 113:027603, Jul 2014.

[7] Joaquin E. Drut and Timo A. Lahde, Is graphene in vacuum an insulator? *Phys. Rev. Lett.*, 102:026802, 2009.

[8] M. V. Ulybyshev *et al.*, Monte-Carlo study of the semimetal-insulator phase transition in monolayer graphene with realistic inter-electron interaction potential. *Phys. Rev. Lett.*, 111:056801, 2013.

[9] D. L. Boyda *et al.*, Many-body effects on graphene conductivity: Quantum Monte Carlo calculations. *Phys. Rev.*, B94(8):085421, 2016.

[10] V. V. Braguta *et al.*, Monte-Carlo study of Dirac semimetals phase diagram. arXiv:1608.07162 [cond-mat.str-el], 2016.

[11] Akihiko Sekine and Kentaro Nomura, Stability of Multinode Dirac Semimetals against Strong Long-Range Correlations. *Phys. Rev.*, B90(7):075137, 2014.

[12] Yasufumi Araki, Lattice gauge theory treatment of strongly correlated Dirac semimetals. *PoS*, LATTICE2015:046, 2016.

[13] J. Gonzalez, Strong-coupling phases of 3D Dirac and Weyl semimetals. A renormalization group approach. *JHEP*, 10:190, 2015.

[14] J. Gonzalez, Phase diagram of the quantum electrodynamics of two-dimensional and three-dimensional Dirac semimetals. *Phys. Rev.*, B92(12):125115, 2015.

[15] Bitan Roy and Sankar Das Sarma. Quantum phases of interacting electrons in three-dimensional dirty dirac semimetals. *Phys. Rev. B*, 94:115137, Sep 2016.

[16] I. Montvay and G. Munster, *Quantum fields on a lattice*. Cambridge University Press, 1997.